

Photorefractive crystal-based holographic interferometry system for full-field wave propagation metrology

Justin D Liou¹, Chih-Kung Lee^{2,3,*}, Kuang-Chong Wu²

¹Department of Electrical Engineering, The Pennsylvania State University,
121 E.E. East Bldg., University Park, PA 16802, U.S.A.

²Institute of Applied Mechanics, National Taiwan University,
1, Sec.4, Roosevelt Rd., Taipei 106, Taiwan

³Department of Engineering Science and Ocean Engineering, National Taiwan University,
1, Sec.4, Roosevelt Rd., Taipei 106, Taiwan

*cklee@ntu.edu.tw

Abstract: Although, photorefractive materials have been discovered for many years, research using pulsed laser as the light source and photorefractive material as the recording media to record a pulsed laser hologram have been scarce despite its vast application potential. A newly proposed optical configuration which adopts a Nd:YAG pulsed laser of 532nm wavelength as the light source and uses an iron-doped lithium niobate crystal as the recording media for holographic recording of an undeformed specimen is presented. Real-time holographic interferometry was achieved by inducing repetitive impacts on the specimen through a precise piezoelectric impact hammer. With timing control better than microseconds, several interferograms created at each instance were obtained with each corresponding 9ns laser pulse. A five-step phase-shifting technology, median filter algorithm, and weighted iterative DFT phase unwrap algorithm were integrated to reconstruct the deformation information at each instance. Using a series of measured deformation data, surface wave propagation phenomenon on the specimen could be observed. Some of the potential applications for this newly developed pulsed laser holographic interferometry system are detailed.

©2007 Optical Society of America

OCIS codes: (090.2880) Holographic Interferometry; (120.2880) Holographic interferometry; (120.4290) Nondestructive testing; (120.7280) Vibration Analysis; (160.5320) Photorefractive materials

References and links

1. R. Aprahamian, "Applications of optical holography to applied mechanics," in *Proceedings of the Engineering Applications of Holography Symposium*, (Feb. 16-17th, 1972), pp. 19-36.
2. A. J. Decker, "Holographic interferometry with an injection seeded Nd:YAG laser and two reference beams," *Appl. Opt.* **29**, 2696-2700 (1990).
3. L. Crawforth, C.-K. Lee, and A. C. Munce, "Application of pulsed laser holographic interferometry to the study of magnetic disk drive component motions," in *Proceedings 1990 International Conference on Hologram Interferometry and Speckle Metrology*, (Nov. 1990), pp. 404-412.
4. Y. Chen, "An ESPI-based Full-field Elastic Wave Propagation Metrology System," Degree Thesis, (National Taiwan University, 2000).
5. U. F. Huang, J. Liou, S. S. Lee, C. K. Lee, and K. C. Wu, "A Full-Field Wave Propagation Pulsed laser Holographic Measurement Technique," in *The First Taiwan-Japan Workshop on Mechanical and Aerospace Engineering*, (Tainan, Taiwan, December 19, 2001), pp. 239-248.
6. A. Ashkin, G. D. Boyd, J. M. Dziedzic, R. G. Smith, A. A. Ballman, J. J. Levinstein, and K. Nassau, "Optically induced refractive index inhomogeneities in LiNbO₃ and LiTaO₃," *Appl. Phys. Lett.* **9**, 72-74 (1966).
7. N. V. Kukharev, V. B. Markov, S. G. Odulov, M. S. Soskin, and V. L. Vinetskii, "Holographic storage in electrooptic crystals. I: steady state," *Ferroelectrics* **23**, 949-960 (1979).
8. N. V. Kukharev, V. B. Markov, S. G. Odulov, M. S. Soskin, and V. L. Vinetskii, "Holographic storage in electro-optic crystals II: beam coupling and light amplification," *Ferroelectrics* **23**, 961-964 (1979).

9. F. S. Chen, J. T. LaMacchia, and D. B. Fraser, "Holographic storage in lithium niobate," *Appl. Phys. Lett.* **13**, 223-225 (1968).
10. T. K. Gaylord, T. A. Rabson, F. K. Tittel, and C. R. Quick, "Pulsed writing of solid state holograms," *Appl. Opt.* **12**, 414-415 (1973).
11. P. Shah, T. A. Rabson, F. K. Tittel, and T. K. Gaylord, "Volume holographic recording and storage in Fe-doped LiNbO₃ using optical pulses," *Appl. Phys. Lett.* **24**, 130-131 (1974).
12. C.-T. Chen, D. M. Kim, and D. von der Linde, "Efficient hologram recording in LiNbO₃: Fe using optical pulses," *Appl. Phys. Lett.* **34**, 321-324 (1979).
13. D. von der Linde, A. M. Glass, and K. F. Rodgers, "Multiphoton photorefractive processes for optical storage in LiNbO₃," *Appl. Phys. Lett.* **25**, 155-157 (1974).
14. R. Magnusson, A. Hafiz, J. S. Bagby, and A. Haji-Sheikh, "Holographic interferometry using self-developing optical crystals for heat flux evaluation," *J. Electron. Packaging.* **122**, 225-259 (1990).
15. X. Wang, R. Magnusson, and A. Haji-Sheikh, "Real-time interferometry with photorefractive reference holograms," *Appl. Opt.* **32**, 1983-1986 (1993).
16. A. Hafiz, R. Magnusson, J. S. Bagby, D. R. Wilson, and T. D. Black, "Visualization of aerodynamic flow fields using photorefractive crystals," *Appl. Opt.* **28**, 1521-1524 (1989).
17. B. Pouet and S. Krishnaswamy, "Dynamic holographic interferometry by photorefractive crystals for quantitative deformation measurements," *Appl. Opt.* **35**, 787-794 (1996).
18. M. P. Georges and P. C. Lemaire, "Phase-shifting real-time holographic interferometry that uses bismuth silicon oxide crystals," *Appl. Opt.* **34**, 7497-7506 (1995).
19. L. Z. Cai, Y. R. Wang, and X. M. Qu, "Wavefront shifting photorefractive holographic interferometer and its applications in optical testing," *Opt. Laser Technol.* **30**, 1-5 (1998).
20. L. Labrunie, G. Pauliat, G. Roosen, and J. C. Launay, "Simultaneous acquisition of $\pi/2$ phase-stepped interferograms with a photorefractive Bi₁₂GeO₂₀ crystal: application to real-time double-pulse holography," *Opt. Lett.* **20**, 1652-1654 (1995).
21. L. Labrunie, G. Pauliat, J. C. Launay, S. Leidenbach, S. Leidenbach, and G. Roosen, "Real-time double exposure holographic phase shifting interferometer using a photorefractive crystal," *Opt. Commun.* **140**, 119-127 (1997).
22. J. P. Huignard, and J. P. Herriau, "Real-time double-exposure interferometry with Bi₁₂SiO₂₀ crystals in transverse electrooptic configuration," *Appl. Opt.* **16**, 1807-1809 (1977).
23. F. Rickermann, S. Riehemann, and G. von Bally, "Utilization of photorefractive crystals for holographic double-exposure interferometry with nanosecond laser pulses," *Opt. Commun.* **155**, 91-98 (1998).
24. C. M. Vest, *Holography Interferometry* (John Wiley & Sons, 1979).
25. D. W. Robinson and G. T. Reid, *Interferogram Analysis: Digital Fringe Pattern Measurement Techniques* (IOP Publishing Ltd., 1993).
26. P. Hariharan, B. F. Orbel, and T. Eiju, "Digital phase-shifting interferometry: a simple error-compensating phase calculation," *Appl. Opt.* **26**, 2504-2507 (1987).
27. C. Rathjen, "Statistical properties of phase-shift algorithms," *J. Opt. Soc. Am. A* **12**, 1997-2008 (1995).
28. C. W. Chen, H. Y. Chang, and C. K. Lee, "An innovative phase shifting system for non-destructive testing," *The Chinese Journal of Mechanics, Series A* **14**, 31-39 (1998).
29. A. Capanni, L. Pezzati, D. Bertani, M. Cetica, and F. Francini, "Phase-shifting speckle interferometry: a noise reduction filter for phase unwrapping," *Opt. Eng.* **36**, 2466-2472 (1997).
30. H. Takajo and T. Takahashi, "Least-squares phase estimation from the phase difference," *J. Opt. Soc. Am. A* **5**, 416-425 (1988).
31. H. Takajo and T. Takahashi, "Noniterative method for the exact solution for the normal equation in least-squares phase estimation from the phase difference," *J. Opt. Soc. Am. A* **5**, 1818-1827 (1988).
32. D. C. Ghiglia and L. A. Romero, "Robust two-dimensional weighted and unweighted phase unwrapping that uses fast transforms and iterative methods," *J. Opt. Soc. Am. A* **11**, 107-117 (1994).
33. *LabVIEW™ User Manual* (National Instruments, Austin, TX, 2000).
34. J. Xie, and Q. Wang, "Analysis and calculation on photorefractive property of Fe:LiNbO₃ crystal," *Optical Technique* **26**, 268-269 (2000).
35. *Quanta-Ray PRO-Series: Pulsed Nd:Yag Lasers User's Manual* (Spectra-Physics, 1999).
36. *PIV: Pulsed Nd:Yag Laser for particle Image Velocimetry User's Manual* (Spectra-Physics, 1997).
37. *Insight™, Particle Image Velocimetry Software, Instruction Manual*, (TSI Incorporated, 2000).
38. C. K. Lee, Paul S. H. Chang, and P. Chang, "Miniature Piezoelectric Actuators: Design Thinking, Fabrication, and Performance Evaluations," *Smart Mater. Struct.* **7**, 312-326 (1998).

1. Introduction

Holographic Interferometry (HI) was first developed to serve as a full-field technique for measuring the static deformation of various structures. Extending this technique to examining the full-field perspective of dynamic or even elastic wave propagation behaviors has always been a research topic that has attracted much attention. However, these kinds of transient phenomena vary rapidly with time and position. The complicated boundary conditions involved in most cases further make numerical solutions difficult to obtain, if not impossible. In this paper, we present a newly developed full-field holographic interferometric technique

that circumvents the difficulties mentioned above and provides us with a route to measure all transient related phenomena.

As early as 1972, Aprahamian [1] tried to apply holographic interferometry to a wave propagation measurement. However, the timing accuracy was not sufficient since a pendulum was used as the impact source. It was not until 1990 that Decker [2] took a twin-cavity Nd:YAG pulsed laser and traditional holographic film to analyze the slit location in the specimen by applying dual-reference and heterodyne configurations. Wet processing for silver halide emulsions and re-positioning to the original place when the hologram was taken was required, which is a very tedious process, not to mention that it is very difficult to reposition the processed silver halide emulsions accurately. Also in 1990, Crawforth *et al.* [3] applied a dual reference and a double exposure holographic interferometry together with a phase-shifting technique to provide a full-field wave propagation metrology by using a twin-cavity high-powered pulsed laser with a Q-switch. To avert the complicated procedures related to film development and precise relocation, DuPont's photopolymer substrate film was introduced by Chen [4] to take advantage of the dry processing steps and to bypass the repositioning requirement. Chen proposed a similar ESPI (Electro-Spackle Interferometry) and holographic interferometry approach. Although, very clear ESPI experimental data were obtained in Chen's work, however, the recorded pulsed images on the photopolymer-based holographic film failed to yield useful data as the photopolymer was not able to react fast enough to the 9ns laser pulses. In 2001, Huang *et al.* [5] uniformly pre-exposed the photopolymer film and recorded the hologram by using the pulsed laser successfully. However, it took dozens of minutes to record the image and to perform the on-site film processing. In addition, the limitation of this process is that a highly stable environment is required. In this paper, photorefractive crystals (PRC) are proposed to replace the photopolymer films previously used due to its higher pulsed laser sensitivity and reusability, and which can also lead to a new full-field wave propagation measurement configuration.

Since photorefractive crystals were discovered in 1966 by Ashkin *et al.* [6], a variety of its phenomena and applications have been published in the literature. In 1979, a Band Transport Model, a well-known model of photorefractive effects, was summarized by Kukhtarev *et al.* [7,8]. A Photorefractive crystal was first used as an erasable holographic recording media by Chen *et al.* [9] in 1968. The photorefractive crystals, also known as PRCs, which are based on volume holography, have attracted much interest due to their dynamic and reversible response to light patterns without further processing. Gaylord *et al.* [10] was the first to record a hologram on an iron-doped lithium niobate crystal by using a pulsed laser. He recorded the holographic image with a pulsed laser but measured its reconstructed diffraction efficiency by using a continuous wave (CW) laser. In 1974, Shah *et al.* [11] used the same approach as that of Gaylord to measure and to propose "photorefractive sensitivity." Chen *et al.*'s experimental set-up [12] showed that the highest photorefractive sensitivity can be obtained at around 30% for iron-doped LiNbO₃ crystals. They also showed that the recorded hologram made by the pulsed laser achieved a photorefractive sensitivity that is one order of magnitude higher than when the hologram is recorded with a CW laser.

As no chemical processing is required to use the photorefractive crystals (PRC) as the recording media, the hologram gratings in the crystal can be gradually erased by using an uniformly distributed read-out beam. Von der Linde *et al.* [13] applied a third uniformly distributed un-frequency-doubled 1060nm light at the same region where the two 530nm beams interfered with each other within the PRC to create the images. He found that the photorefractive sensitivity was clearly enhanced and that the grating formed in the crystal became more difficult to be erased.

Many scholars have adopted PRC with holographic interferometry for several fields of measurements such as those measuring temperature [14, 15], airflow [16], object distortion [17,18] and optical testing [19], etc. Though using PRCs are convenient as no repositioning is required, environment vibrations can affect the results and it remains a major limitation to its application. This disadvantage can be overcome by adopting a pulsed laser instead of a CW laser. Labrunie *et al.* [20, 21] used a Bi₁₂GeO₂₀ crystal and a ruby pulsed laser while

Huignard *et al.*, [22] and Rickermann *et al.*, [23] introduced a pulsed laser and the double-exposure holographic interferometric technique to obtain interferograms to measure the vibration.

As a pulsed laser remains relatively higher in cost and may induce different crystal reaction properties when compared with a CW laser, research on using photorefractive materials as the recording media for pulsed laser holographic interferometry is scarce and remains difficult to implement. In this research, an innovative configuration by using a “real-time” holographic interferometric technique together with an iron-doped lithium niobate crystal and a Nd:YAG pulsed laser, appears to overcome the difficulties mentioned above. We propose this new configuration to visualize not only the vibrations but also the dynamic wave propagation phenomenon.

2. Theory

2.1 Holographic interferometry

As mentioned above, Holographic Interferometry (HI) is a technique that can provide us with an opportunity to understand the deformation of specimens by examining the interference fringe patterns generated. This full-field capability makes HI one of the most important metrology techniques for engineering and industrial applications. Various techniques such as “real-time HI”, “double-exposure HI” and “time-average HI”, etc., have been developed based on holographic interferometric principles over the years to provide full-field metrology functions for engineering applications [24].

The techniques and experimental configurations reported herein can be attributed to a “real-time HI” as a single un-deformed image was recorded by using the photorefractive media first. Each subsequent deformation was taken using a CCD camera to record the interference pattern created from the interference of the reconstructed un-deformed image and the deformed object beam.

2.2 Photorefractive effect

Because of its unique characteristics, photorefractive crystals (PRCs) were used as the holographic interferometric recording media instead of a photopolymer film. To summarize, Kukhtarev’s Band Transport Model described the recording mechanism of two-wave mixing intensity distributions as composed of the following five fundamental processes:

- 1) Impurities are excited and charge carriers are generated due to an intensity distribution,
- 2) Space transportation of these charge carriers are driven by diffusion, drift and photovoltaic effect,
- 3) Trappings of the charge carriers lead to the formation of a space-charge density,
- 4) A photo-induced space charge electric field is formed,
- 5) An index grating is formed via the electro-optic effect.

In our research, we considered various types of photorefractive materials to use in our work. However, we eventually chose an iron-doped LiNbO₃ as the recording media due to its high diffraction efficiency, photorefractive sensitivity, and suitable wavelength.

2.3 Phase-shifting techniques

Since what we obtained on the recording media was not an object deformation information but interference fringes, it was necessary to have a method to evaluate deformation (optical phase) from the interference fringe patterns.

There exists a property termed “direction ambiguity” which essentially states that the direction of the deformation cannot be determined by examining a single holographic interference pattern called an intensity map. More specifically, the entire deformation shape cannot be discerned until the phase map, which represents the optical phase of the

deformation, is retrieved from the intensity map. Phase-shifting is one of the most common techniques available today to obtain the phase information from the interference fringes recorded. By inducing a known phase factor into the optical path so as to modulate the interference fringe images, phase information can be evaluated and the “direction ambiguity” of the interferogram eliminated.

Many techniques including the Carre technique, the three-step technique, and the four-step technique, etc., [25-28] were developed to convert the intensity map to a phase map. In this paper, the five-step technique developed by Hariharan *et al.*, [26] in 1987 was adopted as this particular algorithm was designed to reduce the possibility of having the numerator and denominator become very close zero, which in turn reduces the calculation uncertainty.

Five interference images with relative phase shifts α can be expressed as

$$I_1 = I_0 [1 + \nu \cos(\phi - 2\alpha)] \quad (1)$$

$$I_2 = I_0 [1 + \nu \cos(\phi - \alpha)] \quad (2)$$

$$I_3 = I_0 [1 + \nu \cos \phi] \quad (3)$$

$$I_4 = I_0 [1 + \nu \cos(\phi + \alpha)] \quad (4)$$

$$I_5 = I_0 [1 + \nu \cos(\phi + 2\alpha)] \quad (5)$$

where I_0 is the intensity of the original beam, $I_1 \sim I_5$ are the intensities captured by the CCD camera, ν is the visibility of the fringe patterns, and ϕ is the phase difference of the two incident beams and the item of interest to be measured.

These equations yield

$$\cos \alpha = \frac{I_1 - I_5}{2(I_2 - I_4)} \quad (6)$$

and

$$\tan \phi = \frac{1 - \cos 2\alpha}{\sin \alpha} \times \frac{I_2 - I_4}{2I_3 - I_1 - I_5} \quad (7)$$

In addition, the phase angle ϕ in the form of modulus 2π can be obtained as follows:

$$\phi = \tan^{-1} \left\{ \frac{1 - \cos 2\alpha}{\sin \alpha} \times \frac{I_2 - I_4}{2I_3 - I_1 - I_5} \right\}. \quad (8)$$

As the most significant error factor comes from α , which originates from the phase-shift technique, the five-step technique adopted here reduced the effect of the error. Generally speaking, the more steps adopted in shifting, the less sensitivity to the phase-shift (α) error. Nevertheless, more data certainly leads to a longer computation time as well as a more tedious and time-consuming experimental set-up.

2.4 Median filter

Although the five-step technique is not sensitive to the phase-shifting error, there are still quite a bit of noise which can come from the environment such as dust, air fluctuations, electronic signal transmissions, etc. Pixels tainted by noise can induce errors in calculations during image processing. A proper filter is thus needed to sieve the noises out of the phase images. Many image-filtering algorithms have been developed over the years to remove noise, of which the majority of these algorithms will smooth the discontinuity peaks and valleys. However, for a phase map, these peak-removing algorithms are not applicable since

the peaks and valleys are the most important features in the phase map. The “Median Filter” algorithm developed by Capanni *et al.* [29], which maintains the discontinuity at the phase transition while replacing the noise signal with the expected value in the phase map, was thus adopted to perform the pre-filtering in order to improve the signal-to-noise ratio of the experimental data.

2.5 Phase-unwrapping

Typically, phase unwrapping is used to convert a phase map with values between $(-\pi, \pi]$ into a continuous phase map. Several phase unwrapping algorithms have been previously developed in order to rebuild the phase continuity rather than in the form of modulus of 2π [30-32].

The process that treats a phase-unwrapping task as a solution to a partial differential equation (PDE) in the discrete form was adopted from Ghiglia *et al.* [32]. That is, phase unwrapping ϕ can be viewed as the solution to the following Poisson equation:

$$\frac{\partial^2}{\partial x^2} \phi(x, y) + \frac{\partial^2}{\partial y^2} \phi(x, y) = \rho(x, y) \quad (9)$$

where ϕ is the unwrapped phase and ρ is the algebraic relationship of the pixels around the item of interest, and x and y represent the position of the point. Once the formulation shown in Eq. (9) is adopted, the phase-unwrapping operations can be viewed as the solution to the discrete PDE. Methodologies such as adopting a Discrete Cosine Transform (DCT), Discrete Fourier Transform (DFT), or Fast Fourier Transform (FFT) may be applied to obtain the solution [4, 30, 31]. To facilitate the development as well as future maintenance of this program, LabVIEWTM developed by National Instruments [33] was used as the platform to implement the program. In addition, a “Fourier-transformed-based weighted iterative algorithm” [32] which made the calculations converge to the correct result rather than become affected by the meaningless values in the areas outside of the specimen, was also used to solve the image of non-rectangular objects.

3. Experiment set-up

An iron-doped lithium niobate crystal with 0.05w.t.% Fe_2O_3 doping concentration, of 25x25x4mm in size ordered from CASTECH was used as the recording media. This crystal was selected as it has a relatively larger electro-optic tensor when compared to other kinds of photorefractive crystals and is sensitive to the green region where the 532nm wavelength laser source is located. In this paper, the intersecting angle of the reference beam and the object beam was set at 90 degrees. The optical axis of the crystal was set to the direction of the grating vector, which was 45 degrees. Both angles were regarded as optimal per the results mentioned by Xie *et al.* [34]

3.1 Initial photorefractive crystal response characterization

To obtain the lithium niobate crystal’s characteristics, we first evaluated its diffraction efficiency with two sets of experiments. A 532nm Nd:Yag DiodePump CW laser was used as the light source of the two-wave mixing and to generate interference patterns in the crystal. When the interfering exposure time was long enough to form the saturated index gratings in the crystal, the object beam was blocked and the reference beam then became the only beam incident on the crystal. The diffraction beam intensity as a function of time was recorded continuously starting at the instance when the object beam was blocked. The grating erasure phenomenon could be observed from the diffraction efficiency decaying curves as shown in Fig. 1 and Fig. 2.

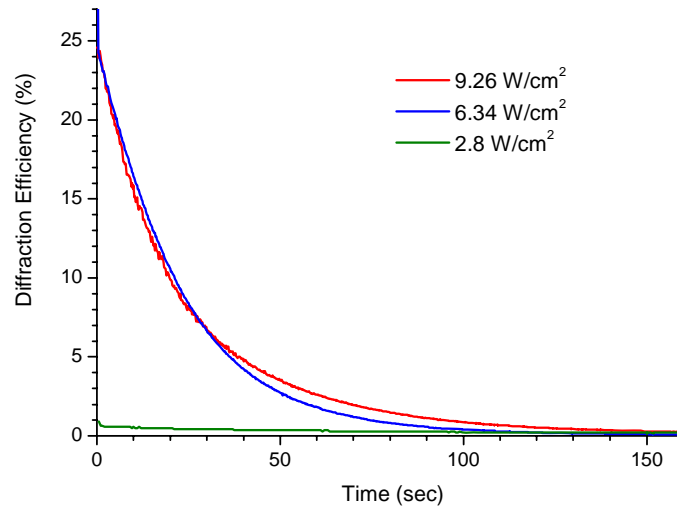


Fig. 1. Index grating erasure under different recording beam intensities

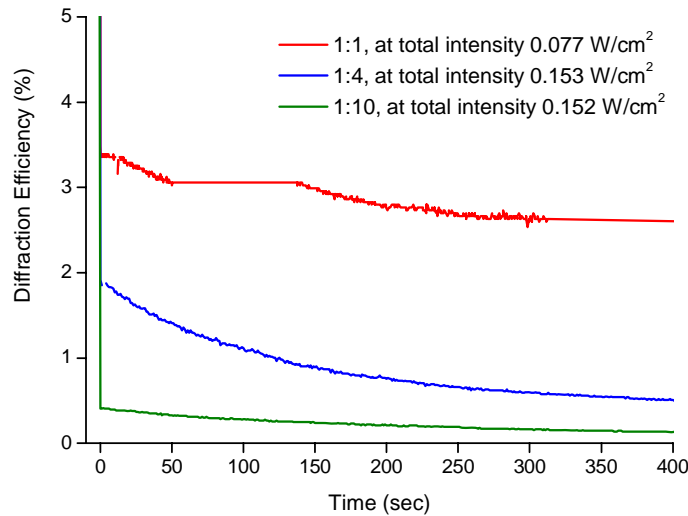


Fig. 2. Index grating erasure under different intensity ratios of reference beams and object beams

With the recording object/reference beam intensity ratio fixed at 1:1 (Fig. 1), we observed that a higher total recording intensity resulted in a higher diffraction efficiency. However, there was an upper saturation limit of this crystal at $\sim 25\%$. We noted that no higher initial diffraction efficiency was obtained when the recording intensity was more than 6 W/cm^2 . In addition, the $1/e$ decay time constants of these three curves were also almost the same ($\sim 25 \text{ sec}$) even for the curve of low intensity at 2.8 W/cm^2 . The exponentially decaying signature of the low intensity case can still be clearly observed when we stretch out the diffraction efficiency axis.

In order to realize if the index modulation of the photorefractive crystals (PRC) can reach its maximum at a non 1:1 object to reference beam intensity ratio as in traditional holographic films (which generally reaches a maximum diffraction efficiency when object to reference intensity ratio is between 1:4 to 1:10, so as to meet the highest slope in its D-E sensitivity curve), several sets of different recording intensity ratios were applied to the crystal. Our results show that 1:1 ratio is still the ideal best condition, even with a lower intensity (Fig. 2). This indicates that no spatial intensity DC term is needed to reach the maximum recording condition. Thus it seems that the highest visibility of interference patterns can result in the highest index modulation. These two fundamental tests provide us with the conditions that we need in the following targeting experiments.

3.2 Dynamic wave-propagation measurement system

The main experimental schematic configuration is shown in Fig. 3. The specimen of interest is a hard disk platter of ~85 mm (3.5") in diameter. As the speed of an elastic wave is about 3000m/sec, the propagation time needed to travel across the specimen for the elastic wave induced by the impact will be less than 50 microseconds. To measure a full-field deformation in such a short period of time, it is important to control the timing accuracy for the image taking up to a micro-second range, which in turn requires a very stable light source. To analyze the surface elastic wave propagation status on the specimen at each instance, a Spectra-Physics PIV-400-15 [35, 36] twin-cavity, injection-seeded frequency-doubled pulsed laser was selected due to its capability of varying the time difference between the two pulses. Furthermore, as this laser adopts two cavities, the time difference that exists between the two pulses, does not affect the intensity of each pulse. The Nd:YAG pulsed laser pumps out a light beam of 1024nm, which then has the frequency doubled to 532nm wavelength by passing through a built-in second harmonic generator.

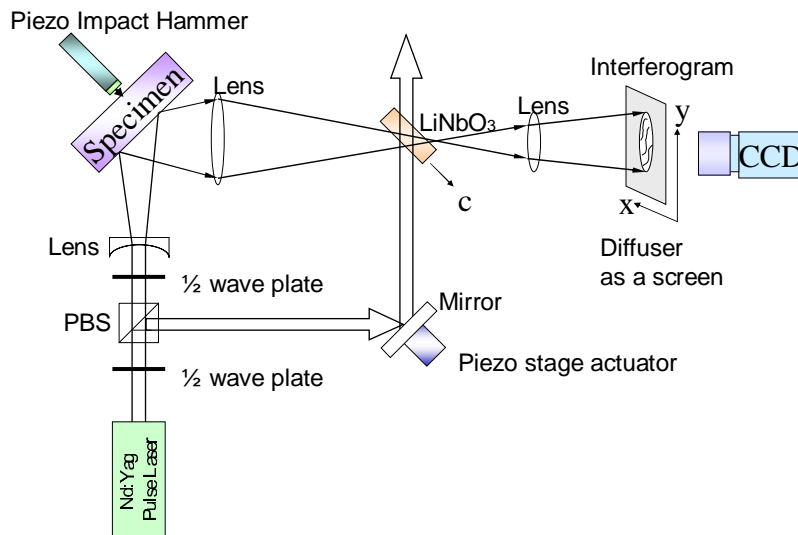


Fig. 3. Schematic of optical experiment set-up

The laser was especially designed to have laser pulses from both cavities mode-locked by reference to a precision He-Ne laser, i.e., the two laser cavities were phase matched by using a PZT actuator to make sure the laser pulses produced by the two cavities possessed the same mode and were able to interfere with respect to each other. A half wave plate was placed inside the laser so as to make these two laser pulses possess an orthogonal polarization orientation. A Q-switch was used to control the pulse spacing. As the normal operating pulse was only 9 ns long, it was short enough to “freeze” each instance of the wave propagation on

the CCD camera. In addition, an alignment mode that generated low power microsecond pulses was also available to facilitate the system set-up. The coherence length of the laser was up to 2m, which is certainly more than enough for the majority of the applications previously mentioned above.

To take advantage of this powerful pulsed laser light source, a PIV (Particle Imaging Velocimetry) CCD Camera PIVCAM10-30 [37] was selected as it can synchronize well with the firing of the twin-cavity laser mentioned above in order to capture the image at the instance when the laser impulse illuminates the object.

By inducing highly repeatable mechanical impact pulses to the specimen, an ultra-precision piezoelectric hammer [38] developed at the Institute of Applied Mechanics, National Taiwan University, was utilized to obtain sub-micrometer positioning accuracy and a sub-microsecond timing accuracy. This specially designed highly repeatable impact hammer was used to make sure that each holographic interferometric data obtained corresponds to different mechanical pulses can be regarded as the result of the same pulse.

A piezoelectric stage was mounted to the back of a mirror located within the reference beam path so as to vary the optical path difference (OPD) between the reference beam and the object beam in order to facilitate phase-shifting operations that convert the intensity maps obtained from the interferogram into phase maps. A synchronizer was connected to a personal computer, which in turn was linked to the impact hammer driving circuits, the twin-cavity laser system, and the CCD image capture system which together triggered all related devices in coherence to obtain the interference fringe images at the correct moment. Figure 4 illustrates the controlling association between the devices.

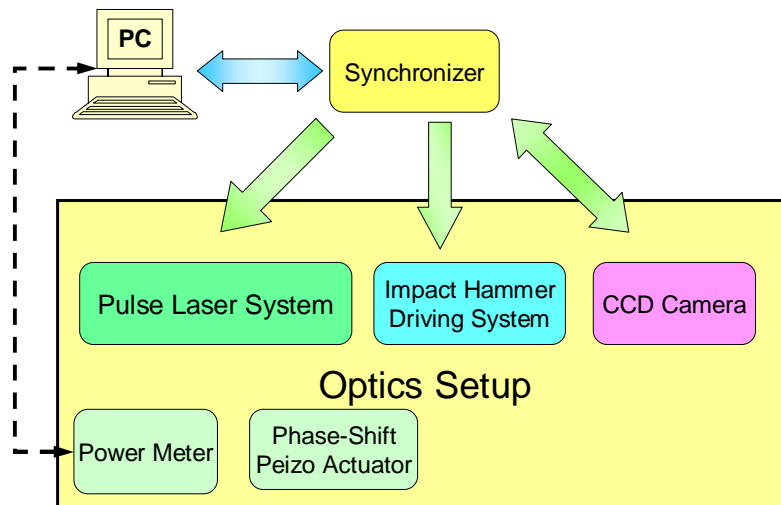


Fig. 4. Schematic for device control & synchronization

Applying a polarizing beam splitter (PBS) and a half wave plate with its fast axis positioned at 45 degrees re-oriented the two orthogonally polarized light beams into the same polarization state. Another angle-tunable half wave plate was positioned in front of the PBS to serve as the mechanism to adjust the intensity ratio between the object and the reference beams. Due to the photorefractive crystal's nonlinear behavior, a mirror-like specimen surface rather than diffusive surface, was chosen so as to make sure enough of the object beam intensity was received by the crystal, i.e., to make sure the light intensity met the index modulation threshold of the crystal.

We found that if the object/reference beam intensity ratio was set at a ratio of 1:1 to a ratio of 1:3 and the total intensity was chosen to be at least 200mW/cm^2 inside the crystal, a clear image of the un-deformed object could be recorded in 2 minutes. This recording time was found to shorten to 50 seconds if light intensity inside the crystal was increased to 280mW/cm^2 . Considering the physics and some earlier results, we believe the recording time can potentially be shortened to a few seconds provided more optimizations were done to parameters such as doping concentration, dopant type, external applied voltage, pulse fluence, etc. Up to a 10% refractive efficiency was achieved by using this 532nm 15 Hz repetitive laser pulses. With no development processes needed for the crystal, an un-deformed image can be reconstructed immediately. However, a relatively lower intensity reference beam must be applied for the sake of not erasing the interferogram grating too quickly.

In summary, the steps adopted included (1) record un-deformed objects by illuminating the photorefractive crystal (PRC) using the interference laser beam up to the grating saturation limit, (2) adjust the object/reference beam ratio to make sure the reconstructed un-deformed image and the deformed image has a 1:1 intensity ratio so as to achieve the best interferogram visibility, (3) adjust the specified time-difference between the hammer impact and the laser firing, (4) trigger the hammer and capture the interferogram images five times with different phase shifts. (5) After obtaining these five intensity maps, apply a five-step phase-shifting technique to retrieve the phase maps, (6) unwrap the phase maps by using a FFT or DCT algorithm to arrive at the deformation maps. Finally, for step (7), repeat steps (3) through step (6) several times with pulses of different time delays. The images-capturing timing sequence is illustrated in Fig. 5 and the image processing procedures can be seen in Fig. 6

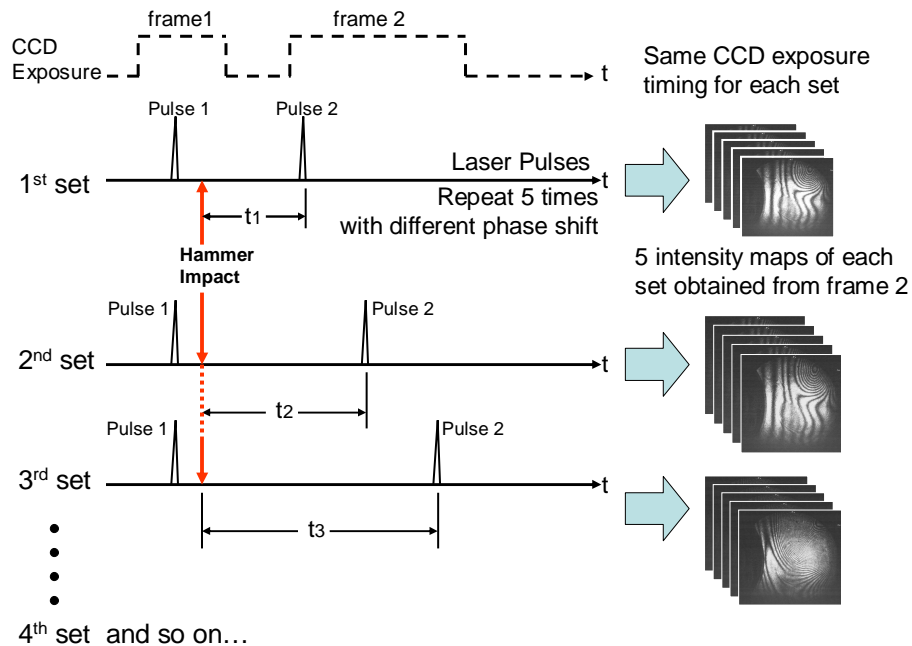


Fig. 5. Laser pulses and image capturing timing sequences. For each set, five slightly different intensity maps captured by Frame 2 were obtained while the time delay between the hammer impact and 2nd pulse was fixed. (Only the images captured by Frame 2 of pulse 2 were adopted in this experiment as pulse 1 was used for triggering and synchronizing purposes.)

The final calculated deformation diagrams with three different time-delays are shown in Fig. 7. From these diagrams, the surface deformation at each instance after the spaceman

undergoes the hammer impact can be clearly visualized and thus the elastic wave propagation behavior can be obtained.

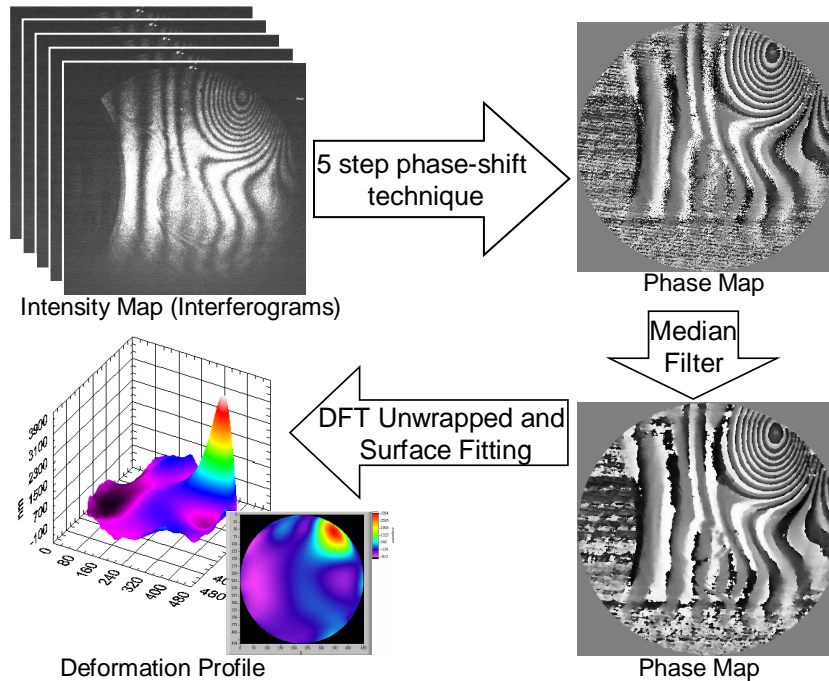
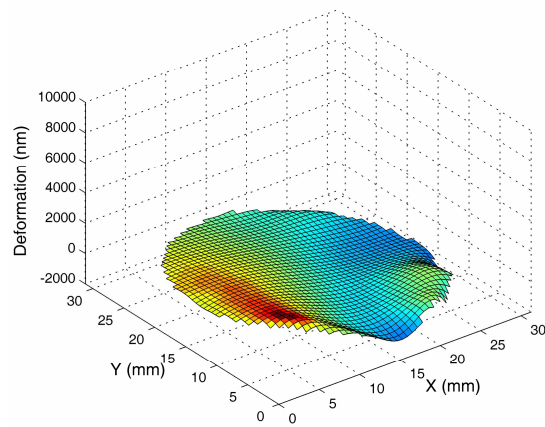


Fig. 6. Image processing procedures from interferograms to unwrapped deformation profiles.

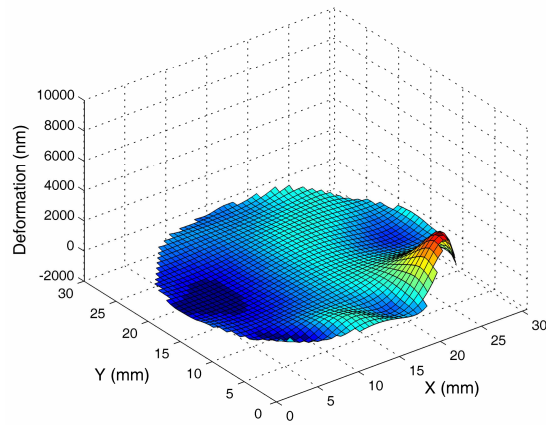
4. Discussions and conclusions

From the above experimental results, it is clear that our experimental set-up is both feasible and practical as depicted by the experimental data shown. The new set-up provides us with a full-field transient elastic wave measurement capability. In addition, it also successfully constructed a new configuration which implemented real-time holographic interferometry in combination with a high power dual-cavity pulsed laser in a photorefractive crystal. The successful incorporation of a newly developed piezoelectric hammer that can induce highly repetitive pluses of precise timing, positioning, and impact loading into the experimental set-up provides us with measurement results that possesses nanometer deformation resolution and a sub-microsecond timing accuracy. Furthermore, by applying the phase-shifting technique, the resolution in an out-of-plane direction can approach up to 2 nanometers and most importantly, the data can be considered to be a full field by the nature of the set-up itself. All in all, this newly developed set-up can be easily adapted to measure elastic wave propagation behavior for various systems of interest.

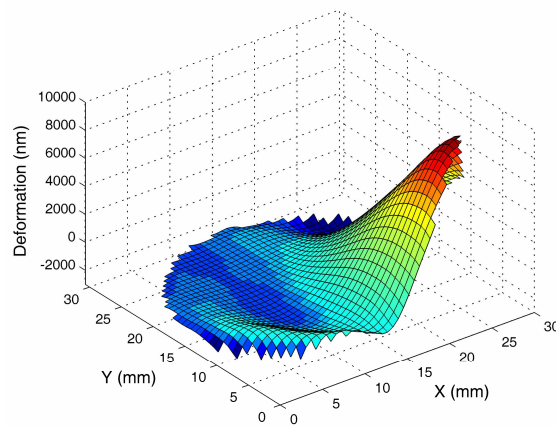
By not using the less-pulse-sensitive photopolymer films and by overcoming the difficulties involved with exposing the photorefractive crystals in a high speed pulsed laser rather than traditional CW laser, this research clearly shows the working conditions for adopting an iron-doped lithium niobate crystal in real-time holographic interferometric applications. By applying the phase-shifting technique, it makes full-field transient measurements applicable and effective. It is expected that this development of the full-field wave propagation measurement technology can be used to measure transient structure deformation, vibration modes, and to find defects, cracks, or areas of concentrated stress, which are of special interest in almost all facets of industries.



(a)



(b)



(c)

Fig. 7. Unwrapped 3D-deformation profiles with different delay times: (a) $5\mu\text{s}$, (b) $10\mu\text{s}$, and (c) $25\mu\text{s}$ after impact by the hammer. Wave growth starting from the impact location can be clearly observed where it is about to propagate through the entire specimen.

Acknowledgments

This research was performed at the Nano-BioMEMS Laboratory at the Institute of Applied Mechanics of National Taiwan University. This project was partially supported under Taiwan's Ministry of Economic Affairs (MOEA), DOIT Technology Development Program for Academia, 95-EC-17-A-05-S1-017 and partially supported by the National Science Council under Project No. NSC 95-2622-E-002-003.